J Physiol 593.8 (2015) pp 2017–2036

The Journal of Physiology

Increased mitochondrial emission of reactive oxygen species and calpain activation are required for doxorubicin-induced cardiac and skeletal muscle myopathy

Kisuk Min[1], Oh-Sung Kwon[1], Ashley J. Smuder[1], Michael P. Wiggs[1], Kurt J. Sollanek[1], Demetra D. Christou[1], Jeung-Ki Yoo[1], Moon-Hyon Hwang[1], Hazel H. Szeto[2], Andreas N. Kavazis[3] and Scott K. Powers[1]

[1]*Department of Applied Physiology & Kinesiology, University of Florida, Gainesville, FL, USA*
[2]*Department of Pharmacology, Weill Cornell Medical College, New York, NY, USA*
[3]*School of Kinesiology, Auburn University, Auburn, AL, USA*

Key points

- Although doxorubicin is a highly effective anti-tumour agent, the administration of this drug is associated with significant side effects, including contractile dysfunction and myopathy of both cardiac and skeletal muscles. The mechanism(s) responsible for doxorubicin-induced contractile dysfunction and myopathy in cardiac and skeletal muscles remains unclear.
- In the present study, we report that increased mitochondrial oxidant production and calpain activation are major contributors to the development of doxorubicin-induced myopathy. Moreover, treatment with a mitochondrial-targeted peptide protects against doxorubicin-induced mitochondrial dysfunction and myopathy in both heart and skeletal muscles.
- These experiments provide insight into the mechanisms responsible for DOX-induced contractile dysfunction and myopathy in cardiac and skeletal muscles. Importantly, our results may provide the basis for developing therapeutic approaches to prevent doxorubicin-induced cardiac and skeletal muscle myopathy.

Abstract Although doxorubicin (DOX) is a highly effective anti-tumour agent used to treat a variety of cancers, DOX administration is associated with significant side effects, including myopathy of both cardiac and skeletal muscles. The mechanisms responsible for DOX-mediated myopathy remain a topic of debate. We tested the hypothesis that both increased mitochondrial reactive oxygen species (ROS) emission and activation of the cysteine protease calpain are required for DOX-induced myopathy in rat cardiac and skeletal muscle. Cause and effect was determined by administering a novel mitochondrial-targeted anti-oxidant to prevent DOX-induced increases in mitochondrial ROS emission, whereas a highly-selective pharmacological inhibitor was exploited to inhibit calpain activity. Our findings reveal that mitochondria are a major site of DOX-mediated ROS production in both cardiac and skeletal muscle fibres and the prevention of DOX-induced increases in mitochondrial ROS emission protects against fibre atrophy and contractile dysfunction in both cardiac and skeletal muscles. Furthermore, our results indicate that DOX-induced increases in mitochondrial ROS emission are required to activate calpain in heart and skeletal muscles and, importantly, calpain activation is a major contributor to DOX-induced myopathy. Taken together, these findings show that increased mitochondrial ROS production and calpain activation are significant contributors to the development of DOX-induced myopathy in both cardiac and skeletal muscle fibres.

DOI: 10.1113/jphysiol.2014.286518

(Received 30 October 2014; accepted after revision 20 January 2015; first published online 23 February 2015)
Corresponding author S. K. Powers: Department of Applied Physiology and Kinesiology, PO Box 118208, University of Florida, Gainesville, FL 32611, USA. Email: spowers@hhp.ufl.edu

Abbreviations 4-HNE, 4-hydroxynoneal; CSA, cross-sectional area; DOX, doxorubicin; ET, ejection time; FS, fractional shortening; IACUC, Institutional Animal Care and Use Committee; IVCT, isovolumic contraction time; IVRT, isovolumic relaxation time; L_o, optimum contractile length; LV, left ventricle; LVDd, left ventricle diameter during diastole; LVDs, left ventricle diameter during systole; MHC, myosin heavy chain; MPI, myocardial performance index; PWSV, left ventricle posterior wall shortening velocity; PWTd, left ventricle posterior wall thickness during diastole; PWTs, left ventricle posterior wall thickness during systole; RCR, respiratory control ratio; ROS, reactive oxygen species; SWTd, septal wall thickness during diastole; SWTs, septal wall thickness during systole; TUNEL, terminal deoxynucleotidyl transferase dUTP nick end labelling.

Introduction

Doxorubicin (DOX) is a highly effective anti-tumour agent and is commonly used in cancer chemotherapy. Unfortunately, the clinical application of DOX is limited by its adverse effects on several tissues, including cardiac and skeletal muscle (Ferrans, 1978; Yamamoto *et al.* 2008; van Norren *et al.* 2009; Gilliam *et al.* 2011). Indeed, one of the most serious side effects of DOX is cardiac damage resulting in the development of cardiomyopathy and, ultimately, congestive heart failure (Jeyaseelan *et al.* 1997; Singal *et al.* 2000). Furthermore, DOX administration at clinical doses results in skeletal muscle weakness, as demonstrated by a decrease in muscle-specific force production (Gilliam *et al.* 2009; Gilliam *et al.* 2011). Therefore, the development of a countermeasure to prevent DOX-induced myopathy in both cardiac and skeletal muscle is important. In this regard, developing a defence against DOX-induced myopathy requires a detailed understanding of the mechanism(s) responsible for DOX-induced damage to both cardiac and skeletal muscles.

It is widely suggested that DOX-induced cardiac and skeletal muscle myopathy occurs as a result of an increased mitochondrial production of reactive oxygen species (ROS) (Berthiaume & Wallace, 2007; Wallace, 2007; Gilliam *et al.* 2011). Specifically, a one-electron reduction of DOX by mitochondrial NADH-dehydrogenase (Complex I) generates the unstable semiquinone, which donates the electron to oxygen, forming the superoxide radical, and it is predicted that the increase in mitochondrial ROS production contributes to DOX-induced cytotoxicity (Doroshow, 1983; Davies & Doroshow, 1986). It has also been hypothesized that DOX-induced increases in ROS production are also linked to increased levels of iron in mitochondria, resulting in a futile redox cycle culminating in increased ROS production and cellular damage (Berthiaume & Wallace, 2007; Ichikawa *et al.* 2014).

In this regard, the treatment of animals with DOX is associated with numerous changes in muscle fibres, including increased mitochondrial ROS production, myonuclear apoptosis, protease activation and contractile dysfunction (Montaigne *et al.* 2011; Carvalho *et al.* 2014). Nonetheless, although it is commonly assumed that mitochondria are the dominant site of ROS production in cardiac and skeletal muscles following DOX administration, it remains to be confirmed experimentally that a DOX-induced increase in mitochondrial ROS emission is required for DOX-induced cardiac or skeletal muscle fibre damage *in vivo*. Therefore, the present study aimed to investigate whether increased mitochondrial ROS emission is essential for DOX-induced myopathy of cardiac and skeletal muscles. In this regard, we utilized the mitochondrial-targeted anti-oxidant SS31, which is preferentially concentrated in the inner mitochondrial membrane (Zhao *et al.* 2004; Doughan & Dikalov, 2007; Anisimov *et al.* 2008). More specifically, SS31 is a multifunctional mitochondrial protective compound that acts by promoting bioenergetics, reducing ROS production, scavenging excess ROS, inhibiting cardiolipin peroxidation and preserving mitochondrial structure (Dai *et al.* 2014).

In addition to increased mitochondrial ROS production, treatment with DOX is also associated with increased activation of the calcium-activated protease calpain (Lim *et al.* 2004). This DOX-induced activation of calpain could occur as a result of oxidative stress-induced increases in cytosolic calcium levels that are required for calpain activation (Goll *et al.* 2003). Increased calpain activity following DOX treatment is potentially important because active calpain degrades >100 cellular proteins including key sarcomeric proteins (Goll *et al.* 2003; Smuder *et al.* 2010) and it has been hypothesized that calpain activation is a key contributor to DOX-induced cardiomyopathy (Campos *et al.* 2011). Nonetheless, experimental evidence to support this assertion is limited.

Therefore, the present study aimed to fill two gaps in our understanding of the mechanism(s) responsible DOX-induced cardiac and skeletal muscle myopathy. Specifically, these experiments tested two integrated hypotheses: (1) prevention of DOX-induced increases in mitochondrial ROS emission will protect against DOX-induced contractile dysfunction and myopathy of cardiac and skeletal muscle fibres and (2) deterrence of calpain activation in cardiac and skeletal muscle myocytes will defend against DOX-induced cardiac and skeletal muscle contractile dysfunction and myopathy. Our results show that increased mitochondrial ROS production and calpain activation are major contributors to the development of DOX-induced myopathy in both cardiac and skeletal muscle fibres.

Methods

Experiment 1

Ethical approval. This experiment tested the hypothesis that increased mitochondrial ROS emission is a requirement for DOX-induced damage and contractile dysfunction in both heart and skeletal muscles. Adult (4- to 6-month-old) female Sprague–Dawley rats were used in this experiment. All animals were housed at the University of Florida Animal Care Services Centre in accordance with guidelines set forth by the Institutional Animal Care and Use Committee (IACUC) and the IACUC approved these experiments prior to their initiation. Animals were maintained under a 12:12 h light/dark cycle and were provided food and water *ad libitum* throughout the experimental period.

Experimental design. Rats were randomly assigned to one of four groups ($n = 8$ group^{-1}): (1) control animals injected with saline (CON); (2) animals injected with DOX (DOX); (3) control animals injected with the mitochondrial-targeted anti-oxidant SS31 (CON + SS31); and (4) animals injected with DOX and SS31 (DOX + SS31).

DOX and DOX + SS31 animals received a single I.P. injection of DOX hydrochloride (20 mg kg^{-1} of body weight) 48 h prior to being killed (Pfizer, New York, NY, USA). This dose of DOX is a human clinical dose of this drug that is pharmacologically scaled for use in rats (Yen *et al.* 1996; Kang *et al.* 1997; Childs *et al.* 2002). The peptide SS31 was chosen as the mitochondrial-targeted anti-oxidant in our experiments because it freely crosses cell membranes and enters the mitochondria to selectively targets cardiolipin on the mitochondrial inner membrane (Zhao *et al.* 2004; Birk *et al.* 2013). Importantly, SS31 promotes oxidative phosphorylation and reduces mitochondrial ROS production (Zhao *et al.* 2004; Birk *et al.* 2014). The CON + SS31 and DOX + SS31 animals received daily I.P. injections of SS31 (3 mg kg^{-1}) beginning 24 h prior to treatment with DOX (Stealth Peptides, Newton Centra, MA, USA).

Following the assigned treatments, animals were anaesthetized with gaseous isoflurane (3% for induction; 1.5–2.5% for maintenance) and anaesthetized animals were used to obtain echocardiographic measurements (the time of anaesthesia was maintained constant for all animals at 20 min). Next, the heart, diaphragm, soleus and plantaris muscles were removed and used for analyses. Specifically, small pieces of left ventricle, diaphragm, soleus and plantaris muscles were permeabilized to measure mitochondria function and ROS emission. A strip of diaphragm was immediately used for *in vitro* contractile measurements. Also, small pieces of left ventricle, diaphragm, soleus and plantaris were stored for histological measurements. The remaining portions of the left ventricle, diaphragm, soleus and plantaris were rapidly frozen in liquid nitrogen and stored at –80°C for subsequent biochemical analyses.

Experiment 2

Animals. This experiment tested the hypothesis that calpain activation is a major contributor to DOX-induced cardiac and skeletal muscle myopathy. Adult (4- to 6-month-old) female Sprague–Dawley rats were used in this experiment and received housing/feeding treatment identical to that for animals in Experiment 1. The IACUC of the University of Florida also approved these experiments prior to their initiation.

Experimental design. Rats were randomly assigned to one of four groups ($n = 8$ group^{-1}): (1) control animals injected with saline (CON); (2) animals injected with DOX (DOX); (3) control animals injected with the calpain inhibitor SJA 6017 (SJA) (CON + SJA); and (4) animals injected with DOX and SJA (DOX + SJA).

DOX and DOX + SJA animals received a single I.P. injection of DOX hydrochloride (20 mg kg^{-1} of body weight) 48 h prior to being killed. SJA is a peptide inhibitor of calpain (Calpain inhibitor IV; EMD Chemicals, Gibbostown, NJ, USA). Although many of the catalytic site-directed peptidyl calpain inhibitors lack intracellular specificity, plasma membrane permeability and potency, the permeability of SJA across cell membranes is relatively high compared to other widely used inhibitors (Fukiage *et al.* 1997). The therapeutic efficacy of SJA to inhibit calpain activation is well established (Fukiage *et al.* 1997; Kupina *et al.* 2001; Sharma & Rohrer, 2004). Animals assigned to SJA treatment received a daily I.P. injection of SJA (3 mg kg^{-1}) for 3 days. The first SJA injection was performed 24 h prior to DOX treatment. Animals were anaesthetized with gaseous isoflurane (3% for induction; 1.5–2.5% for maintenance) and anaesthetized animals were used to obtain echocardiographic measurements (the time of anaesthesia was maintained constant for all animals at 20 min). Following completion of these experiments, the heart, diaphragm, soleus and plantaris muscles were removed and used for analyses, as described previously.

Echocardiography

Transthoracic echocardiography was performed using an ultrasound system (Aplio XV; Toshiba Medical Systems, Tokyo, Japan) equipped with a 7.5 MHz transducer. Two-dimensional ultrasound images and M-mode tracings of the left ventricle (LV) were obtained in the parasternal short-axis view at the level of the papillary muscles. Measurements were then performed using the leading edge to leading edge technique: LV diameter during diastole (LVDd) and systole (LVDs), septal wall thickness during diastole (SWTd) and systole (SWTs), LV posterior wall thickness during diastole (PWTd) and systole (PWTs). Fractional shortening (FS), an index used to assess LV systolic function, was calculated as (LVDd − LVDs)/LVDd × 100%. LV posterior wall shortening velocity (PWSV), another measure of LV systolic function, was also measured. Pulsed-wave Doppler of mitral flow velocity was recorded in the apical four-chamber view with the smallest sample volume placed at the tips of the mitral valve. The myocardial performance index (MPI), an index used to assess combined diastolic and systolic function, was calculated as (IVCT + IVRT)/ET, where IVCT is the isovolumic contraction time, IVRT is the isovolumic relaxation time and ET is the ejection time. Measurements of diameters, thicknesses and time intervals were performed on five to 10 cardiac cycles and averaged for each rat.

Preparation of permeabilized muscle fibres

Approximately 25 mg of heart, diaphragm, soleus and plantaris muscles were dissected and placed on a plastic Petri dish containing ice-cold buffer X (60 mM K-Mes, 35 mM KCl, 7.23 mM K_2EGTA, 2.77 mM CaK_2EGTA, 20 mM imidazole, 0.5 mM dithiothreitol, 20 mM taurine, 5.7 mM ATP, 15 mM PCr and 6.56 mM $MgCl_2$, pH 7.1). The muscle was then cut down to fibre bundles (4–8 mg wet weight). The muscle fibre bundles were gently separated in ice-cold buffer X to maximize surface area of the fibre bundle. To permeabilize the myofibres, each fibre bundle was incubated in ice-cold buffer X containing 50 μg ml^{-1} saponin for heart, soleus and plantaris muscles and 75 μg ml^{-1} saponin for diaphragm muscle on a rotator for 30 min at 4°C. The permeabilized muscle bundles were then washed in ice-cold buffer Z (110 mM K-Mes, 35 mM KCl, 1 mM EGTA, 5 mM K_2HPO_4, and 3 mM $MgCl_2$, 0.005 mM glutamate, 0.02 mM malate and 0.5 mg ml^{-1} BSA, pH 7.1).

Mitochondrial respiration and ROS emission

Respiration was measured polarographically in a respiration chamber maintained at 37°C (Hanstech Instruments, King's Lynn, UK). After the respiration chamber was calibrated, permeabilized fibre bundles were incubated with 1 ml of respiration buffer Z containing 20 mM creatine to saturate creatine kinase. Flux through complex I was measured using 5 mM pyruvate and 5 mM malate. The ADP-stimulated respiration (state 3) was initiated by adding 0.25 mM ADP to the respiration chamber. Basal respiration (state 4) was determined in the presence of 10 μg ml^{-1} oligomycin to inhibit ATP synthesis. The respiratory control ratio (RCR) was calculated by dividing the state 3 by state 4 respiration.

ROS emission in permeabilized muscle fibres was determined using Amplex Red (Molecular Probes, Eugene, OR, USA). Details of this assay have been described previously (Min *et al.* 2011). Briefly, this assay is based on the concept that HRP catalyses the H_2O_2-dependent oxidation of non-fluorescent Ampex Red to fluorescent resorufin red. Superoxide dismutase was added to the preparation to convert all superoxide into H_2O_2. Although this assay measures all H_2O_2 produced in the fibre, previous work predicts that the majority of ROS production in the permeabilized muscle fibre preparation is released from mitochondria within the skeletal muscle fibres (Anderson & Neufer, 2006; Anderson *et al.* 2009). Mitochondrial ROS production was measured during state 3 respiration using the creatine kinase energy clamp technique to maintain respiration at a steady state using methods described previously (Messer *et al.* 2004).

Diaphragmatic contractile properties

A diaphragm strip including the tendinous attachments at the central tendon and rib cage was dissected from the mid-costal region. The strip was suspended vertically between two lightweight plexiglas clamps with one end connected to an isometric force transducer (model FT-03; Grass Instruments, Quincy, MA, USA) within a jacketed tissue bath. The force output was recorded via a computerized data-acquisition system (Super Scope II; GW Instruments Somerville, MA, USA; Apple Computer, Cupertino, CA, USA). The tissue bath was filled with Krebs-Hensleit saline and the buffer was aerated with gas (95% O_2/5% CO_2), pH was maintained at 7.4, and the osmolality of the bath was ~290 mosmol (kg H_2O)$^{-1}$. After a 15 min equilibration period (25°C), *in vitro* diaphragmatic contractile measurements were made. The muscle strip was stimulated along its entire length with platinum wire electrodes (modified S48 stimulator; Grass Instruments) using a supramaximal (~150%) stimulation voltage to determine the optimum contractile length

(L_o). L_o was determined by systematically adjusting the length of the muscle using a micrometer while evoking single twitches. Thereafter, all contractile properties were measured isometrically at L_o. To measure maximal isometric twitch force, each strip was stimulated supramaximally with 120 V pulses at 1 Hz and, to measure the force frequency response, each strip was stimulated supramaximally with 120 V pulses at 15–160 Hz. The duration of each train was 500 ms to achieve a force plateau. Contractions were separated by a

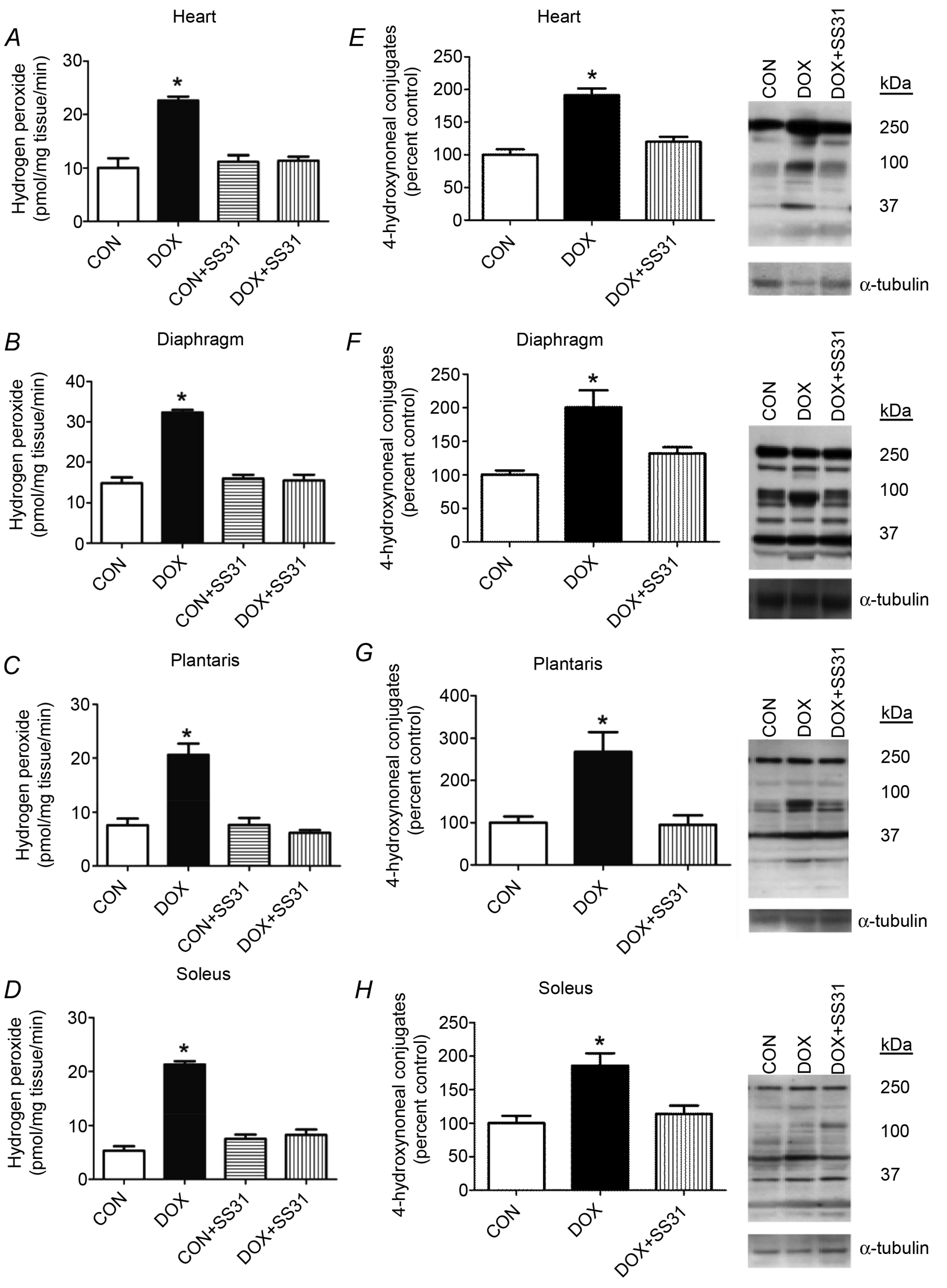

Figure 1. Hydrogen peroxide release and oxidative damage in heart and skeletal muscles
A–D, rates of hydrogen peroxide release from permeabilized cardiac and skeletal muscle fibres. Values are the mean ± SEM. *DOX significantly different *vs.* CON, CON + SS31 and DOX + SS31 ($P < 0.05$). *E–H*, 4-hydroxynonenal conjugates were analysed as an indicator of lipid peroxidation. Representative western blot images of 4-hydroxynonenal are shown to the right. *DOX significantly different *vs.* CON and DOX + SS31 ($P < 0.05$).

2 min recovery period. For comparative purposes, diaphragmatic (bundles of fibres) force production was normalized as specific tetanic force. The total muscle cross-sectional area at right angles to the long axis was calculated by the following algorithm (Segal *et al.* 1986). Total muscle cross-sectional area (mm^2) = [muscle mass / (fibre length × 1.056)], where 1.056 is the density of muscle (in g cm^3). Fibre length was expressed in centimeters measured at L_o (Reid, 2008).

Myofibre cross-sectional area

Sections from diaphragm, soleus and plantaris samples were cut at 10 μm with a cryotome (Shandon Inc., Pittsburg, PA, USA) and allowed to air dry at room temperature for 30 min. For fibre cross-sectional area (CSA), sections were stained for dystrophin (red), myosin heavy chain (MHC) I (blue) and MHC IIa (green), and all remaining unstained fibres (black) were classified as MCH IIb/x, as described previously (McClung *et al.* 2007). The CSA was determined using Scion software (NIH, Bethesda, MD, USA).

Western blot analysis

Protein abundance was determined in heart, diaphragm, soleus and plantaris samples via western blot analysis. Briefly, tissue samples were homogenized 1:10 (w/v) in 5 mM Tris (pH 7.5) and 5 mM EDTA (pH 8.0) with a protease inhibitor cocktail (Sigma, St Louis, MO, USA) and centrifuged at 1500 *g* for 10 min at 4°C. After the resulting supernatant was collected, the protein content was assessed by the method of Bradford

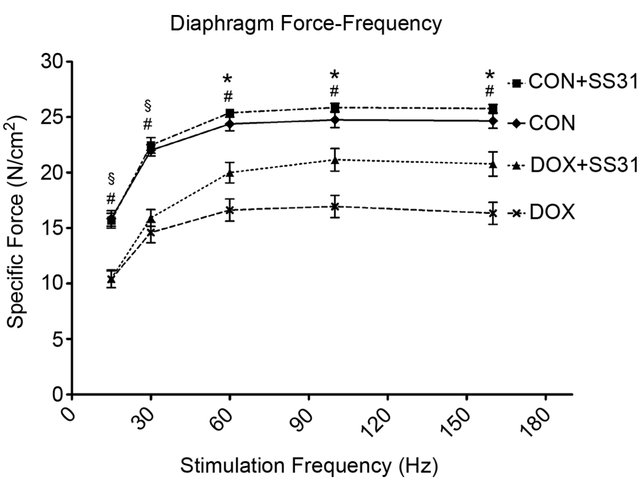

Figure 2. Diaphragm force-frequency response in all experimental groups
Values are the mean ± SEM. §DOX significantly different *vs.* CON and CON + SS31 ($P < 0.05$). *DOX significantly different *vs.* CON, CON + SS31 and DOX + SS31 ($P < 0.05$). #DOX + SS31 significantly different *vs.* CON and CON + SS31 ($P < 0.05$).

(Sigma). Proteins from the supernatant fraction were separated by PAGE via 4–20% gradient polyacrylamide gels containing 0.1% SDS. After electrophoresis, the proteins were transferred to nitrocellulose membranes and incubated with primary antibodies [4-hydroxynoneal (4-HNE); #ab46545; Abcam, Cambridge, MA, USA; calpain 1, #2556; Cell Signaling Technology, Carlsbad, CA, USA] directed against proteins of interest.

Following incubation with primary antibodies, membranes were washed extensively with PBS-Tween and then incubated with secondary antibodies (GE Healthcare, Piscataway, NJ, USA). After being washed, a chemiluminescence system was used to detect labelled proteins (GE Healthcare). Membranes were developed using autoradiography film and images of the film were captured and analysed using the 440CF Kodak Imaging System (Kodak, New Haven, CT, USA). Proteins located down the entire lane were used for 4-HNE analysis, and the autolysis product (75 kDa) of calpain 1 was evaluated as a biomarker of calpain activity. Alpha-tubulin (Santa Cruz Biotechnology, Santa Cruz, CA, USA) was analysed to provide a control for protein loading.

Assay of caspase-3 activity

Caspase-3 activity was measured using the Caspase-Glo assay system (Promega, Madison, WI, USA). Briefly, samples were homogenized 1:10 (w/v) in 5 mM Tris·HCl and 5 mM EDTA (pH 7.5) without the addition of a protease inhibitor cocktail and centrifuged at 10000 *g* for 10 min at 4°C. The resulting supernatant was collected and protein content was assessed by the Bradford method (Sigma). Approximately 50 μg of protein was incubated with a caspase-3 specific cleavage product and bioluminescence intensity was measured by plate reader, and final values were normalized to the total protein input.

TUNEL

Myonuclear apoptosis was determined by TUNEL using a histochemical fluorescence detection kit (Roche Applied Scientific, Indianapolis, IN, USA). Briefly, 10 μm tissue sections were fixed using in a 4% formaldehyde solution, washed, and permeabilized with 0.1% Triton X-100 in 0.1% sodium citrate solution. For identification of cell membranes, tissues were incubated with a rabbit anti-dystrophin antibody (Thermo Scientific; Freemont, CA, USA) and secondary conjugated to Rhodamine Red (Invitrogen, Eugene, OR, USA). Tissue sections were then incubated with the TUNEL enzyme label solution and sealed with a Vectashield 4′,6-diamidino-2-phenylindole mounting medium for detection of nuclei (Vector Laboratories, Burlingame, CA, USA). TUNEL stained tissue sections were imaged using a fluorescence microscope (Zeiss, Thornwood, NY, USA). Fluorescence images for 4′,6-diamidino-2-phenylindole (nuclei), rhodamine (dystrophin) and fluorescein isothiocyanate filters (TUNEL positive) were combined using IPLab software (Scanalytics, Inc., Fairfax, VA, USA). TUNEL positive nuclei were counted and normalized to tissue cross-sectional area.

Statistical analysis

Comparisons between groups were made by ANOVA. When appropriate, Tukey's honestly significant diference *post hoc* test was performed to identify differences between groups. $P < 0.05$ was considered statistically different.

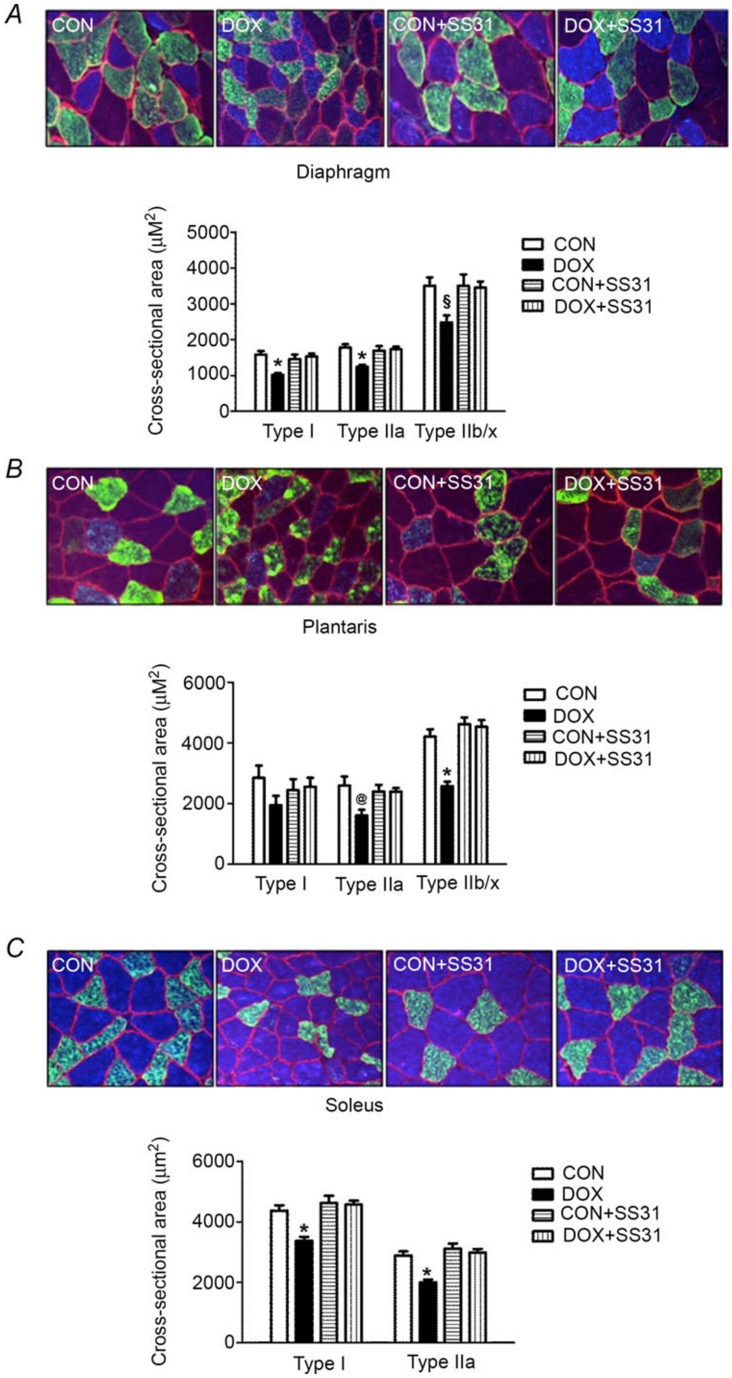

Figure 3. Fibre cross-sectional area of diaphragm, plantaris and soleus
A) diaphragm, *B*) plantaris and *C*) soleus. Values are the mean ± SEM. *DOX significantly different *vs.* CON, CON + SS31 and DOX + SS31 ($P < 0.05$). §DOX significantly different *vs.* CON and CON + SS31 ($P < 0.05$). @DOX significantly different *vs.* CON ($P < 0.05$). Representative images are shown at the top. Fibre membranes are highlighted by dystrophin stain (red). Fibre types can be identified as MHC I (blue) and MHC IIa (green), and all remaining fibres were classified as MCH IIb/x (black).

Table 1. Mitochondrial respiratory function in permeablized fibre from heart and diaphragm for Experiment 1

Heart	CON	DOX	CON ± SS31	DOX ± SS31
State 3 respiration	15.7 ± 0.59	13.4 ± 0.59*	17.3 ± 1.19	16.8 ± 0.93
State 4 respiration	3.5 ± 0.24	4.3 ± 0.18	3.6 ± 0.29	3.7 ± 0.27
RCR	4.7 ± 0.39	3.2 ± 0.25†	5.0 ± 0.55	4.8 ± 0.59
Diaphragm				
State 3 respiration	14.9 ± 1.09	10.2 ± 0.44†	16.0 ± 1.04	13.3 ± 0.63
State 4 respiration	3.9 ± 0.12	3.7 ± 0.19	4.2 ± 0.33	3.8 ± 0.27
RCR	3.9 ± 0.31	2.5 ± 0.15†	4.0 ± 0.51	3.6 ± 0.20

Values are expressed as the mean ± SEM. *DOX significantly different *vs.* CON + SS31 and DOX + SS31 ($P < 0.05$). †DOX significantly different *vs.* CON and CON + SS31 ($P < 0.05$). State 3 and State 4 respiration (oxygen consumption) is expressed as pmol (mg tissue)$^{-1}$ min^{-1}.

Table 2. *In vivo* cardiac function and wall thickness measures from Experiment 1

	CON	DOX	CON ± SS31	DOX ± SS31
FS (%)	50.39 ± 1.09	29.85 ± 0.36*	49.50 ± 0.75	45.44 ± 1.13†
PWSV (mm s^{-1})	31.34 ± 0.37	22.06 ± 0.84*	30.33 ± 0.82	29.09 ± 0.60
MPI	0.47 ± 0.05	1.04 ± 0.11*	0.39 ± 0.04	0.69 ± 0.03‡
SWTd (mm)	1.46 ± 0.02	1.28 ± 0.06*	1.46 ± 0.02	1.45 ± 0.03
SWTs (mm)	2.72 ± 0.05	2.08 ± 0.06*	2.55 ± 0.03	2.53 ± 0.04§
PWTd (mm)	1.43 ± 0.04	1.24 ± 0.04*	1.48 ± 0.03	1.45 ± 0.03
PWTs (mm)	2.54 ± 0.05	2.01 ± 0.07*	2.58 ± 0.07	2.40 ± 0.04

Values are expressed as the mean ± SEM. *DOX significantly different *vs.* CON, CON + SS31 and DOX + SS31 ($P < 0.05$). †DOX + SS31 significantly different *vs.* CON and CON + SS31 ($P < 0.05$). ‡DOX + SS31 significantly different *vs.* CON + SS31 ($P < 0.05$). §DOX + SS31 significantly different *vs.* CON ($P < 0.05$).

Results

Experiment 1

This experiment determined whether increased mitochondrial ROS production is a requirement for DOX-induced myopathy in both cardiac and skeletal muscles. Cause and effect was established by using a novel mitochondrial-targeted anti-oxidant (SS31) to prevent DOX-induced increases in mitochondrial ROS emission.

SS31 protects against DOX-induced increases in mitochondrial ROS emission and mitochondrial damage in both cardiac and skeletal muscles

Because mitochondria are predicted to be a major source of DOX-induced ROS production in cells, we determined the effect of the mitochondrial-targeted anti-oxidant SS31 on DOX-induced ROS emission from cardiac and skeletal muscles (Fig. 1*A–D*). Our data show that DOX treatment resulted in significant increases in mitochondrial ROS emission in both cardiac and skeletal muscles (i.e. diaphragm, soleus and plantaris muscles) and, importantly, treatment of animals with SS31 prevents DOX-mediated mitochondrial ROS emission in these tissues (Fig. 1*A–D*).

To determine whether SS31 protects both cardiac and skeletal muscle mitochondria from DOX-induced mitochondrial uncoupling, the mitochondrial RCR was measured. DOX administration significantly reduced the RCR in cardiac and diaphragm skeletal muscle compared to CON. Note that treatment of CON animals with SS31 did not significantly alter any variable measured (Figs 1*A–D*, 2 and 3; Tables 1 and 2,). Furthermore, although treatment with SS31 tended to attenuate the DOX-induced mitochondrial uncoupling, this protection did not reach statistical significance (Table 1). To determine whether mitochondrial ROS production is responsible for oxidative damage to muscle proteins following DOX administration, 4-HNE was measured as a biomarker of lipid peroxidation in both heart and skeletal muscles. Compared to CON, DOX administration resulted in a significant increase in 4-HNE modified proteins in cardiac and skeletal muscles (Fig. 1*E–H*). Importantly, treatment of animals with SS31 prior to DOX administration protected the heart and skeletal muscles against DOX-induced increases in 4-HNE.

Taken together, these findings reveal that increased mitochondrial ROS emission is a requirement for DOX-induced mitochondrial uncoupling and oxidative damage in both cardiac and skeletal muscle.

SS31 prevents DOX-induced cardiac contractile dysfunction and atrophy

To determine the effect of DOX treatment on cardiac function *in vivo*, indices of LV systolic and diastolic function were measured using echocardiography (Table 2). Compared to control, DOX administration resulted in an ∼41% decline in FS (i.e. a measure of systolic function). Importantly, SS31 administration attenuated the DOX-induced decline in FS ($P < 0.05$). In addition, DOX treatment decreased another index of systolic function (i.e. PWSV) by ∼30%, whereas treatment with SS31 prior to DOX administration protected against the DOX-induced decrease in PWSV ($P < 0.05$). Furthermore, compared to CON, DOX treatment decreased MPI (i.e. measure of diastolic and systolic function) by ∼120%. Importantly, treatment of animals with SS31 attenuated the DOX-induced detrimental effects on MPI ($P < 0.05$).

To determine the effect of DOX treatment on cardiac wall thickness *in vivo*, septal and LV posterior wall thickness were measured using echocardiography. DOX administration resulted in thinning of both SWT and PWT during systole (24% and 21%, respectively) and diastole (12% and 13%, respectively) (Table 2). However, when animals were treated with SS31 prior to DOX administration, the DOX-induced thinning of the septal and LV posterior walls was prevented (Table 2). Finally, treatment of control animals with SS31 did not alter any of the cardiac function or wall thickness measures.

SS31 prevents DOX-induced skeletal muscle contractile dysfunction and atrophy

Similar to the effects of DOX on cardiac muscle, DOX administration also promotes skeletal muscle contractile dysfunction and atrophy. Thus, we measured diaphragmatic contractile properties (i.e. force–frequency response) to determine the effectiveness of SS31 in preventing DOX-induced skeletal muscle contractile dysfunction. Our results reveal that DOX administration significantly reduced diaphragmatic specific force production compared to CON animals at all stimulation frequencies (Fig. 2). Importantly, treatment with SS31 protected against DOX-induced diaphragm contractile dysfunction at stimulation frequencies greater than 30 Hz ($P < 0.05$).

To determine whether SS31 can protect against DOX-induced skeletal muscle atrophy, myofibre CSA was evaluated in diaphragm, soleus and plantaris muscles. Specifically, sections were stained for dystrophin (red), MHC I (blue) and MHC IIa (green). All remaining unstained fibres (black) were classified as MCH IIb/x. DOX administration resulted in a significant decrease in fibre CSA (Fig. 3). However, treatment with SS31 prior to DOX administration protected against DOX-induced atrophy in the diaphragm (type I and type IIa), plantaris (type IIb/x) and soleus (type I and type IIa). Finally, treatment of control animals with SS31 was not found to alter skeletal muscle fibre CSA (Fig. 3).

SS31 prevents protease activation and apoptosis in the heart and skeletal muscles of animals treated with DOX

To determine whether DOX-induced increases in mitochondrial ROS emission are required to activate calpain in cardiac and skeletal muscle, calpain 1 autolysis (i.e. the 75 kDa autolysis product of calpain 1) was used as a biomarker of calpain activation (Saido *et al.* 1994). Because our results (heart and diaphragm mitochondrial respiration and ROS emission, cardiac function by echocardiography, diaphragmatic contractile properties, and myofibre cross-sectional area) did not indicate any differences between CON and CON + SS31, the samples for CON + SS31 were not analysed; therefore, all results are reported as CON *vs.* all other experimental groups. Our results reveal that activation of calpain was increased in cardiac and skeletal muscle following DOX administration, whereas treatment with SS31 prevented this DOX-induced increase in calpain activation in both cardiac and skeletal muscle (Fig. 4*A*–*D*).

Caspase-3 is a protease capable of degrading intact actomyosin proteins and it also plays a key role in promoting myonuclear apoptosis in muscle fibres (Smuder *et al.* 2010). Compared to control animals, DOX administration resulted in a significant increase in caspase-3 activity in cardiac muscle along with the diaphragm and plantaris muscles. Importantly, treatment with SS31 prevented DOX-induced increases in caspase-3 activity in cardiac muscle along with the diaphragm and plantaris muscles (Fig. 4*E*–*H*). Unexpectedly, caspase-3 was not active at the time of assay in soleus muscle of the DOX-treated animals. Nonetheless, based upon TUNEL-positive nuclei measurements (see below), caspase-3 was probably active in the soleus muscle of the DOX-treated animals at some point following the administration of DOX.

Again, because activation of caspase-3 can lead to apoptosis, histological sections from both cardiac and skeletal muscle were evaluated to determine the number of TUNEL-positive nuclei as an index of apoptosis. Our data demonstrate that DOX administration resulted in a significant increase in the number of TUNEL-positive nuclei in both cardiac and skeletal muscles of DOX treated animals. However, treatment with SS31 prevented DOX-induced increases in apoptosis in the heart and skeletal muscles (Fig. 5*A*–*D*).

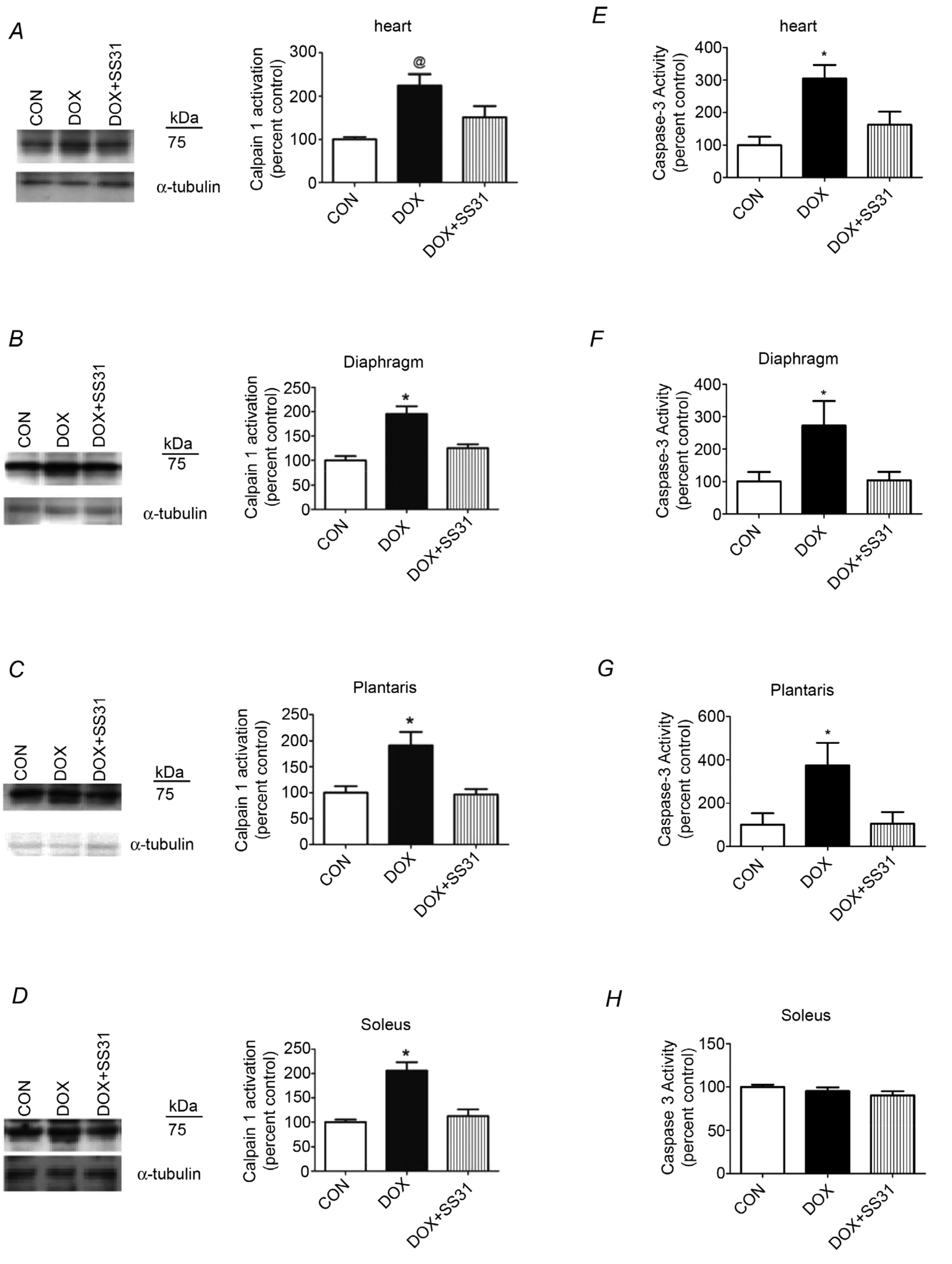

Figure 4. Calpain and caspase-3 activation in heart and skeletal muscles
A–*D*, calpain activation [autoproteolytic product (75 kDa) of calpain 1] in heart and skeletal muscles. *E*–*H*, Caspase-3 activation in heart and skeletal muscles. *DOX significantly different *vs.* CON and DOX + SS31 ($P < 0.05$). @DOX significantly different *vs.* CON ($P < 0.05$). Representative western blot images are shown to the left.

Experiment 2

This experiment investigated the role that calpain activation plays in DOX-induced cardiac and skeletal muscle myopathy. Cause and effect was determined using the specific calpain inhibitor SJA 6017.

Inhibition of calpain activation attenuates DOX-induced cardiac and skeletal muscle contractile dysfunction and atrophy

Identical to Experiment 1, compared to control animals, DOX administration resulted in impairments in cardiac

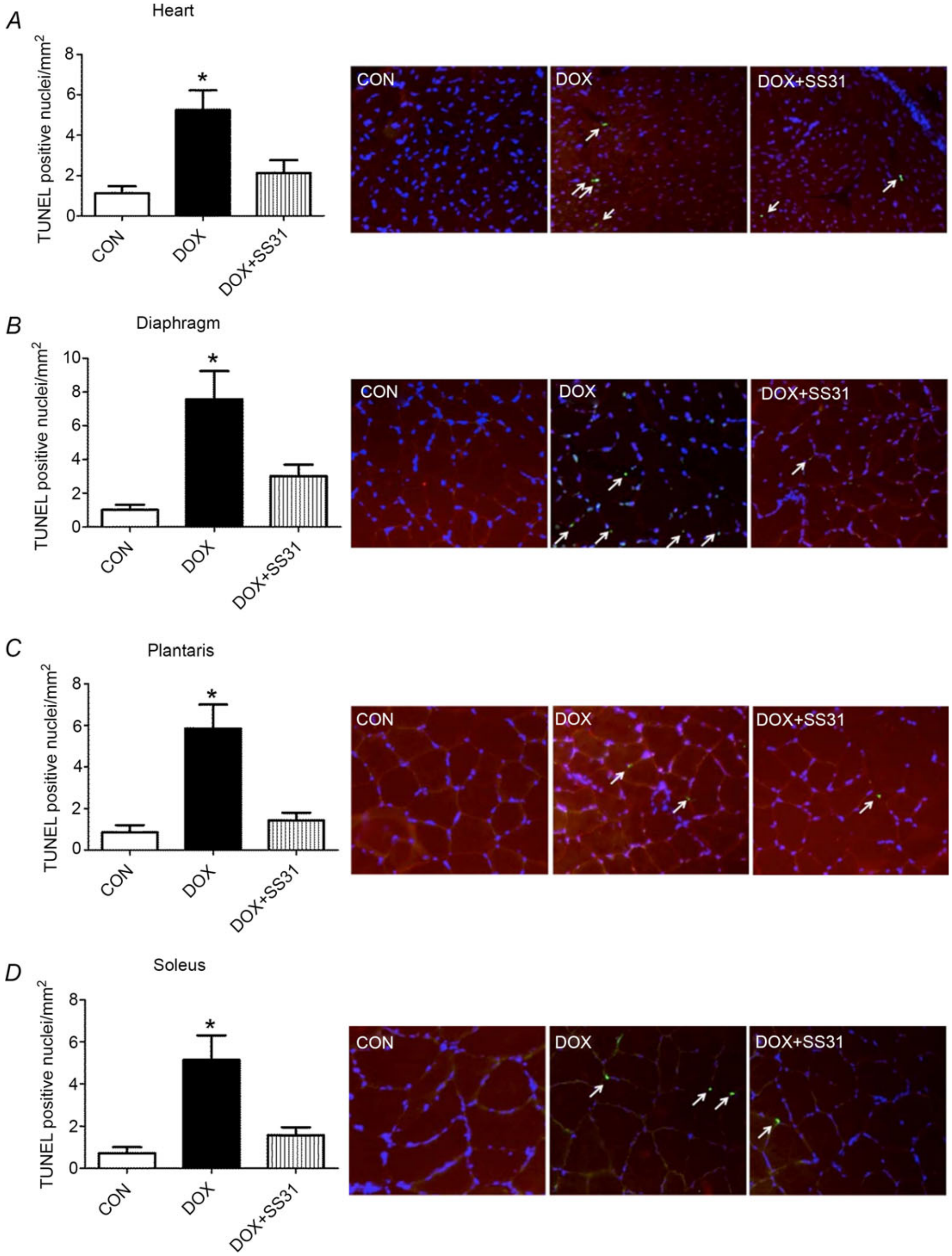

Figure 5. Number of positive TUNEL nuclei in heart and skeletal muscles
A) heart, *B*) diaphragm, *C*) plantaris and *D*) soleus. *DOX significantly different *vs.* CON and DOX + SS31 ($P < 0.05$). The arrows indicate TUNEL positive nuclei. Representative images are shown to the right.

Table 3. *In vivo* cardiac function and wall thickness measures from Experiment 2

	CON	DOX	CON±SJA	DOX±SJA
FS (%)	49.91 ± 1.10	35.48 ± 1.16*	47.29 ± 1.34	41.82 ± 0.91§
PWSV (mm/sec)	30.23 ± 1.28	22.69 ± 073†	29.08 ± 2.51	25.53 ± 0.57
MPI	0.41 ± 0.03	0.92 ± 0.08†	0.39 ± 0.04	0.78 ± 0.05§
SWTd (mm)	1.54 ± 0.04	1.34 ± 0.06†	1.56 ± 0.03	1.43 ± 0.03
SWTs (mm)	2.76 ± 0.08	2.29 ± 0.04*	2.63 ± 0.07	2.54 ± 0.04
PWTd (mm)	1.63 ± 0.05	1.32 ± 0.06†	1.56 ± 0.03	1.43 ± 0.03‡
PWTs (mm)	2.66 ± 0.04	2.19 ± 0.04†	2.68 ± 0.05	2.36 ± 0.05§

Values are expressed as the mean ± SEM. *DOX significantly different *vs.* CON, CON + SJA and DOX + SJA ($P < 0.05$). †DOX significantly different *vs.* CON and CON + SJA ($P < 0.05$). ‡DOX + SJA significantly different *vs.* CON ($P < 0.05$). §DOX + SJA significantly different *vs.* CON and CON + SJA ($P < 0.05$).

function, as indicated by the significant decline in FS and PWSV, thinning of the septal and LV posterior wall, and a significant decrease in MPI (Table 3). Inhibition of calpain activation via SJA attenuated the DOX-induced decline in FS and SWTs. Importantly, short-term (i.e. 72 h) treatment of control animals with SJA did not significantly alter any of these cardiac measures.

Treatment with SJA prior to DOX injections also attenuated the DOX-induced decline in diaphragm contractile dysfunction (Fig. 6). Specifically, compared to CON, DOX administration resulted in a significant reduction in the specific force production of diaphragm muscle at all stimulation frequencies. However, prevention of DOX-induced calpain activation provided significant protection against DOX-mediated decreases in diaphragm muscle force production at 30 Hz. Also, compared to DOX treatment alone, animals treated with both SJA and DOX tended to have higher diaphragmatic specific force production at stimulation frequencies >30 HZ, albeit no significant differences existed. Notably, treatment of control animals with SJA did not alter diaphragm force production at any stimulation frequency.

Myofibre CSA was evaluated to determine the role of active calpain on DOX-induced skeletal muscle atrophy. Treatment with DOX resulted in a significant decrease in muscle fibre CSA in type I, type IIa and type IIx/b in the diaphragm, plantaris and soleus muscles (Fig. 7*A*–*C*). Importantly, inhibition of calpain activity protected against DOX-induced atrophy in diaphragm (type I), plantaris (type IIa) and soleus muscle (type I and type IIa fibres) (Fig. 7*A*–*C*). Finally, treatment of control animals with SJA did not alter fibre CSA in any muscle group.

DOX-induced caspase-3 activation and apoptosis is reduced by SJA

Because our results (cardiac function by echocard-iography, diaphragmatic contractile properties and myofibre cross-sectional area) did not indicate differences between CON and CON + SJA, the samples for CON + SJA were not analysed; therefore, all results are reported as CON *vs.* all other experimental groups. As previously discussed, DOX administration results in a significant increase in active calpain 1 in both heart and skeletal muscles and treatment with SJA was successful in preventing DOX-induced increases in the activation of calpain in both heart and skeletal muscles (Fig. 8*A*–*D*).

Active calpain has been shown to activate caspase-3 in skeletal muscle (Nelson *et al.* 2012) and active caspase-3 can degrade myofibrillar proteins. Therefore, active caspase-3 can contribute to DOX-induced muscle myopathy (Kavazis *et al.* 2010; Smuder *et al.* 2011). Compared to control animals, DOX administration resulted in a significant increase in cleaved (active) caspase-3 in cardiac and skeletal muscles (i.e. diaphragm and plantaris) (Fig. 8*E*–*H*). Although DOX treatment tended to increase caspase-3 activity in the soleus muscle,

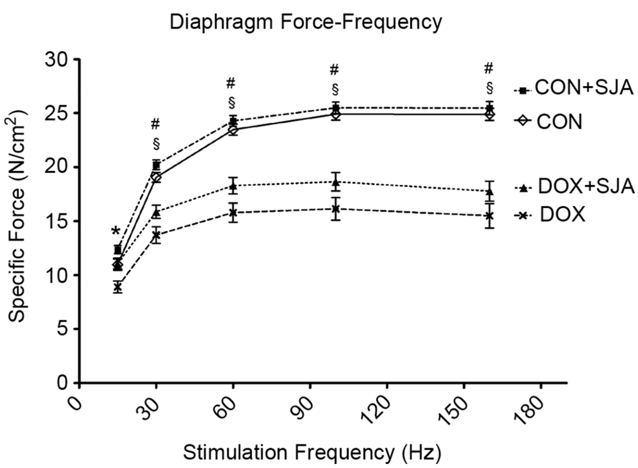

Figure 6. Diaphragm force-frequency response
Values are the mean ± SEM. *DOX significantly different *vs.* CON, CON + SJA and DOX + SJA ($P < 0.05$). #DOX + SJA significantly different *vs.* CON and CON + SJA ($P < 0.05$). §DOX significantly different *vs.* CON and CON + SJA ($P < 0.05$).

this increase did not reach significance. Furthermore, DOX administration resulted in a significantly higher number of TUNEL-positive nuclei in both cardiac and skeletal muscles (Fig. 9*A–D*). Notably, treatment with SJA prevented DOX-induced increases in caspase-3 activity and also prevented the increase in myonuclear apoptosis in cardiac and skeletal muscles (Fig. 8*E–H* and Fig. 9*A–D*).

Discussion

Overview of principal findings

These experiments provide novel insight into the mechanisms responsible for DOX-induced contractile dysfunction and myopathy in both cardiac and skeletal muscle. Our findings confirm that mitochondria comprise

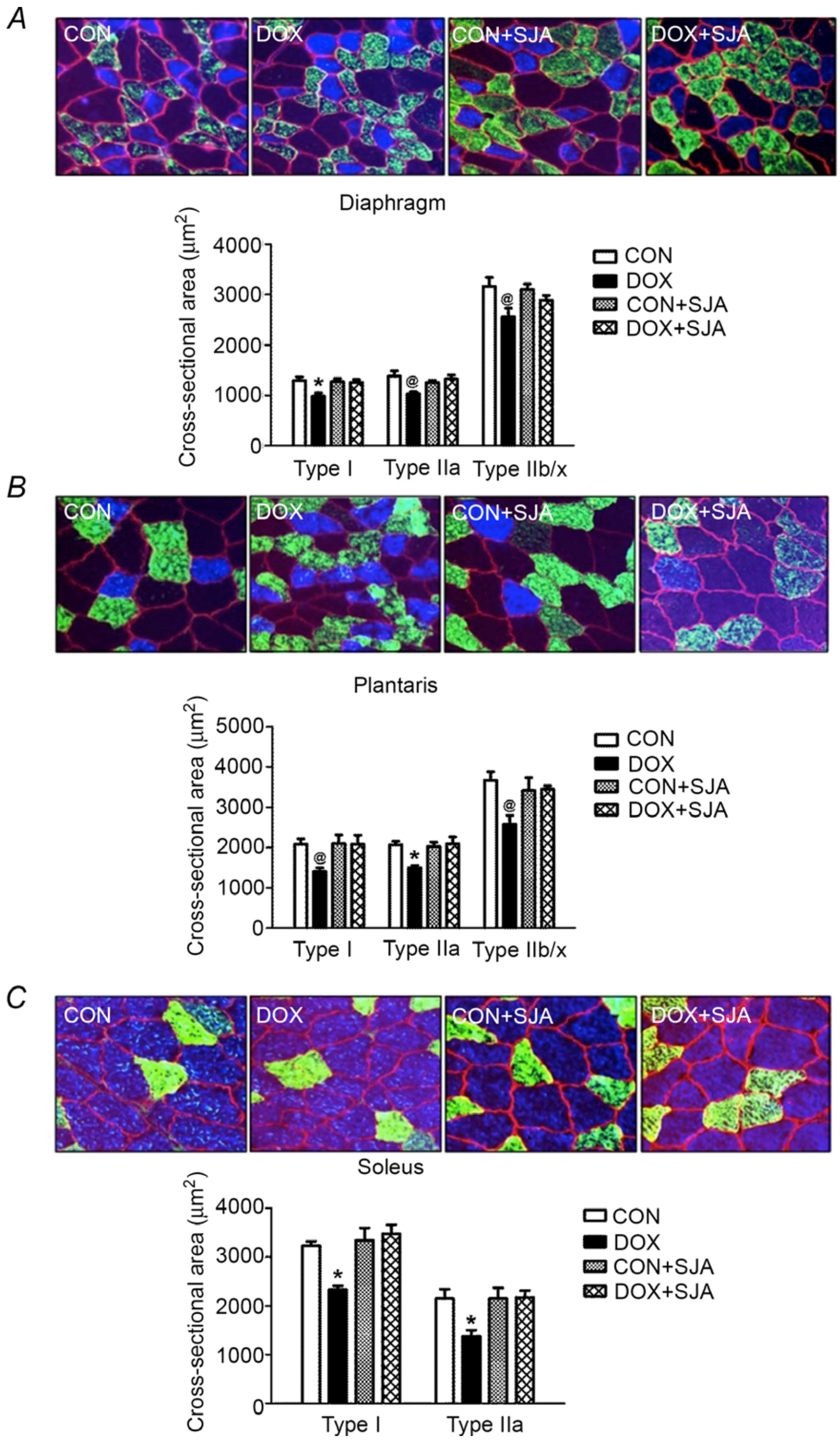

Figure 7. Cross-sectional area of diaphragm, plantaris and soleus
A) diaphragm, *B*) plantaris and *C*) soleus. Values are the mean ± SEM. *DOX significantly different *vs.* CON, CON + SJA, and DOX + SJA ($P < 0.05$). @DOX significantly different *vs.* CON ($P < 0.05$). Representative images are shown at the top. Fibre membranes are highlighted by dystrophin stain (red). Fibre types can be identified as MHC I (blue) and MHC IIa (green), and all remaining fibres were classified as MCH IIb/x (black).

a dominant site of DOX-mediated ROS production in both cardiac and skeletal muscle fibres and that treatment with the mitochondrial-targeted peptide SS-31 prevents DOX-induced increases in mitochondrial ROS emission and also protects against mitochondrial damage, fibre atrophy and contractile dysfunction in both cardiac and skeletal muscles. Furthermore, our results reveal that a DOX-induced increase in mitochondrial damage and ROS emission are required to activate calpain in heart and skeletal muscles. Finally, our findings confirm that calpain

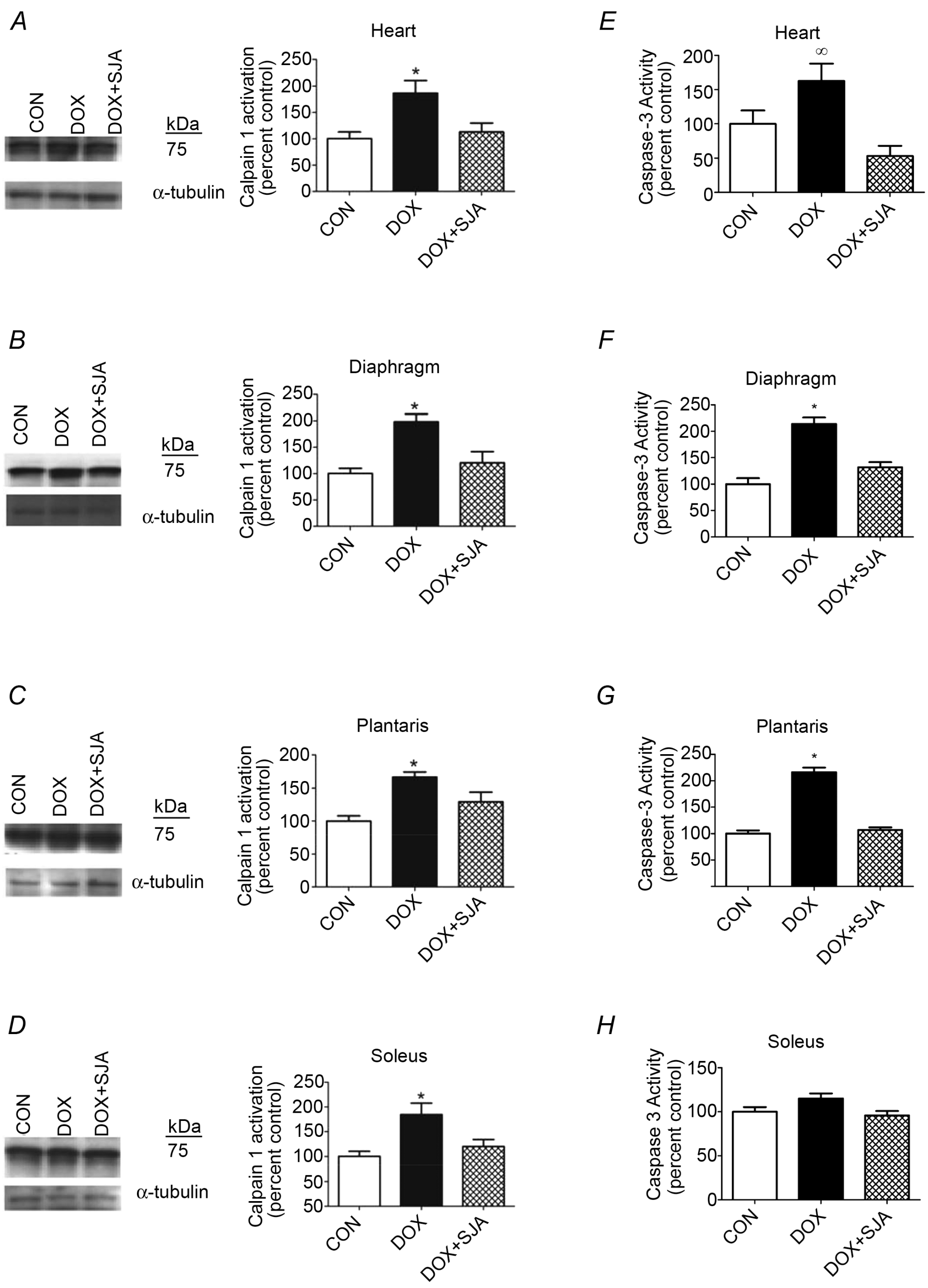

Figure 8. Calpain and caspase-3 activation in heart and skeletal muscles
A–D, calpain activation [autoproteolytic product (75 kDa) of calpain 1] in heart and skeletal muscles. *E–H*, Caspase-3 activation in heart and skeletal muscles. *DOX significantly different *vs.* CON and DOX + SJA ($P < 0.05$). ∞DOX significantly different *vs*. DOX + SJA. Representative Western blot images are shown to the left.

activation is a key contributor to DOX-induced myopathy. A detailed discussion of these findings is provided below.

DOX administration results in cardiac and skeletal muscle dysfunction

Doxorubicin is a widely used and highly effective anti-tumour agent. However, its clinical application is limited as a result of the severe cardiac toxicity associated with DOX treatment. Indeed, our data confirm that DOX administration rapidly results in a severe cardiomyopathy and DOX-induced toxicity is not limited to cardiac tissue because specific force production is also significantly reduced in the principal inspiratory muscle (i.e. diaphragm) as a result of DOX treatment. Moreover,

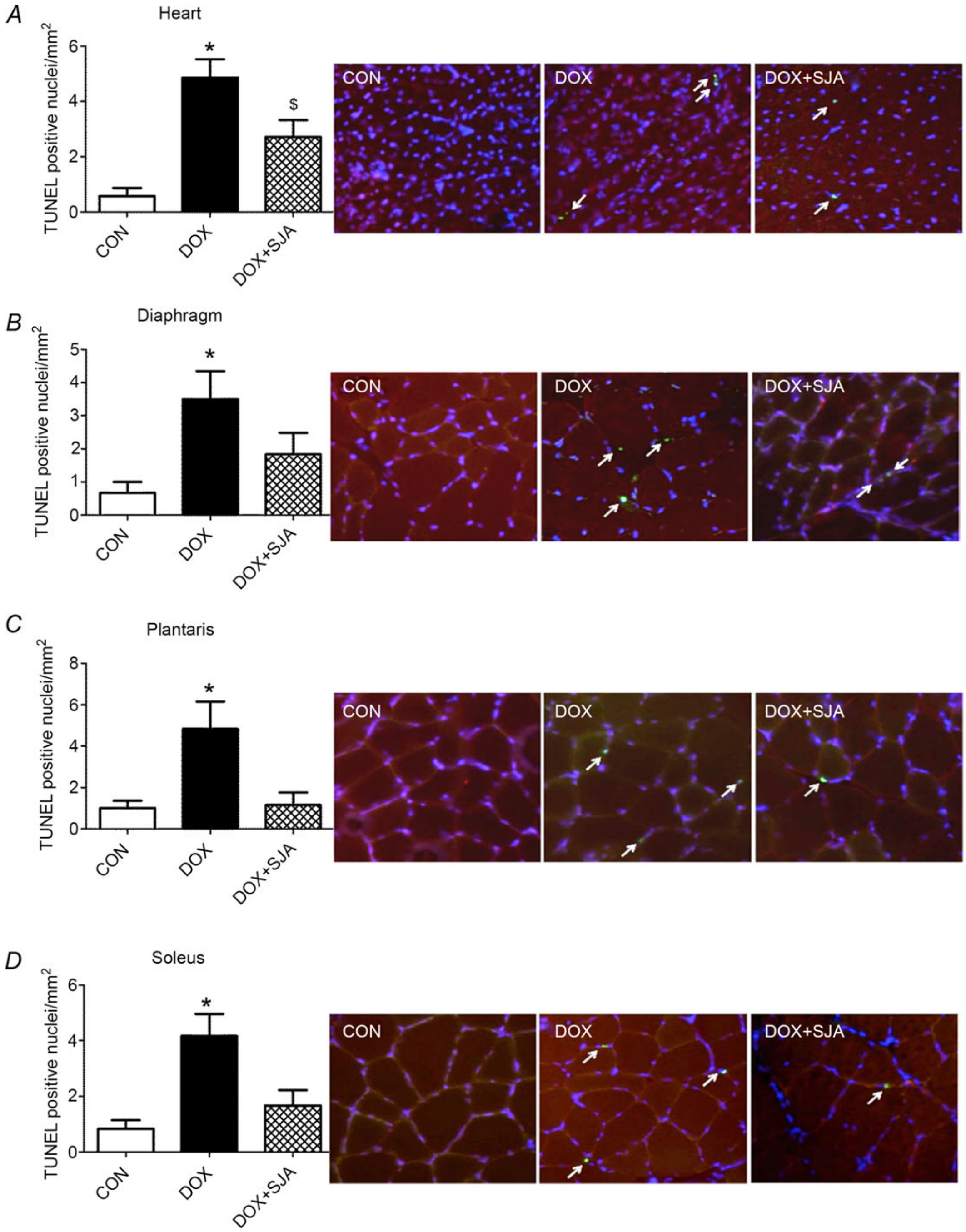

Figure 9. Number of positive TUNEL nuclei in heart and skeletal muscles
A) heart, *B*) diaphragm, *C*) plantaris and *D*) soleus. *DOX significantly different *vs.* CON and DOX + SJA ($P < 0.05$). $DOX + SJA significantly different than CON ($P < 0.05$). The arrows indicate TUNEL positive nuclei. Representative images are shown to the right.

our findings agree with previous work indicating that treatment of animals with DOX also results in the rapid development of muscle fibre atrophy in diaphragm and limb skeletal muscles (Gilliam *et al.* 2009; Gilliam *et al.* 2011; Hayward *et al.* 2013).

Increased mitochondrial ROS production is required for DOX-induced myopathy

It is well established that DOX administration results in the increased formation of ROS, mitochondrial damage, and oxidative damage to cardiac and skeletal muscles fibres (Myers *et al.* 1977; Singal *et al.* 1997; Wonders *et al.* 2009; Montaigne *et al.* 2011; Smuder *et al.* 2011). In addition, the DOX-induced inhibition of mitochondrial ATP production has been recognized as another potential mechanism contributing to DOX toxicity (Tokarska-Schlattner *et al.* 2006). Specifically, studies of mitochondrial respiration in rat skeletal muscles reveal that a decrease in state 3 respiration occurs rapidly (i.e. within 2 h) following DOX administration and this impairment of electron transport is sustained for at least 72 h (Gilliam *et al.* 2013). The results of the present study support these earlier results and also confirm that DOX administration results in a decrease in state 3 respiration and increased mitochondrial uncoupling in both cardiac and diaphragm muscle fibres. This DOX-induced disruption of electron flow is probably another source of oxidant production and contributes to the overall mitochondrial oxidant damage associated with DOX treatment.

The inhibitory action of DOX on the electron transport chain is probably caused by the binding of DOX to cardiolipin, a phospholipid located on the inner mitochondrial membrane that is essential for maintaining cellular bioenergetics (Goormaghtigh *et al.* 1986; Goormaghtigh *et al.* 1990). The binding of DOX to cardiolipin can alter fluidity and folding of the cristae membranes and impair the function of the electron transport chain. Indeed, there are numerous reports of DOX inhibiting function of the mitochondrial respiratory complexes (Goormaghtigh *et al.* 1986; Tokarska-Schlattner *et al.* 2006; Chandran *et al.* 2009). This DOX-mediated damage of numerous components of the electron transport chain results in electron leak and increased ROS formation (Pfeiffer *et al.* 2003). Furthermore, cardiolipin is readily peroxidized in an oxidant environment and cardiolipin peroxidation results in the inhibition of mitochondrial respiration and also induces the opening of the mitochondrial transition pore. Indeed, exposure to DOX increases the sensitivity of skeletal and cardiac muscle to mitochondrial pore opening (Montaigne *et al.* 2011; Gilliam *et al.* 2013). Therefore, collectively, DOX administration is associated with increased mitochondrial ROS production, inhibition of the electron transport chain and increases the risk of mitochondrial permeability transition (Wallace, 2007).

The results of the present study show that mitochondrial damage and increased mitochondrial ROS emission are required for DOX-mediated oxidative damage in both cardiac and skeletal muscles. Unequivocally, our results reveal that DOX administration results in increased mitochondrial ROS emission. Importantly, treatment with the mitochondrial-targeted anti-oxidant SS31 protects both cardiac and skeletal muscles against DOX-induced increased mitochondrial ROS emission, and also prevents DOX-induced oxidative damage to proteins. The exact mechanism of how SS31 prevents DOX-induced increases in mitochondrial ROS emission and damage is not clear, although at least two major possibilities exist. First, SS31 is known to bind with high affinity to cardiolipin (Birk *et al.* 2013) and therefore may displace the binding of DOX to cardiolipin. By contrast to DOX, the interaction of SS31 with cardiolipin facilitates electron transfer through the cytochrome *c*–cardiolipin complex and improves the efficiency of the electron transport chain (Birk *et al.* 2014). Second, SS31 can attenuate DOX-induced mitochondrial ROS formation by scavenging electrons (Zhao *et al.* 2004). Regardless of the primary mechanism responsible for SS31-mediated protection against DOX-induced mitochondrial damage, our results are consistent with the concept that increased mitochondrial damage and elevated ROS emission are primary contributors to DOX-induced oxidative damage in cardiac and skeletal muscles.

Following these findings, we then investigated several downstream targets of ROS that can contribute to DOX-induced cellular damage. Specifically, we studied calpain and caspase-3 activation because these proteases can be activated by oxidant stress (Whidden *et al.* 2010; Powers *et al.* 2011*a*) and both proteases contribute to disuse muscle atrophy (Nelson *et al.* 2012). Our findings confirm that DOX administration increases the activity of both calpain and caspase-3 in cardiac and skeletal muscles and, importantly, treatment with the mitochondrial-targeted anti-oxidant SS31 protects against DOX-induced activation of these proteases. To our knowledge, these are the first experiments to show that increased mitochondrial ROS emission is essential for DOX-induced activation of both calpain 1 and caspase-3 in cardiac and skeletal muscles.

Although our experiments do not reveal the mechanism(s) linking increased mitochondrial ROS emission to the activation of calpain and caspase-3, increased mitochondrial ROS emission can elevate cytosolic free calcium via several mechanisms, including ROS-mediated calcium release from the sarcoplasmic reticulum and decreased calcium removal from the cell as a result of oxidative damage to calcium transporters located in the plasma membrane (Powers *et al.* 2011*b*;

Powers *et al.* 2012*b*). Increased cellular free calcium is important because elevated cytosolic levels of calcium are required to activate both calpain 1 and 2 in the cytosol (Goll *et al.* 2003). Moreover, increased cytosolic free calcium combined with increased mitochondrial ROS production can promote caspase-3 activation via mitochondrial-mediated pathways (Powers *et al.* 2007; Powers *et al.* 2012*a*). Also, new evidence reveals that a regulatory interaction exists in skeletal muscle whereby active calpain can trigger caspase-3 activation and active caspase-3 can enhance calpain activation via a cross-talk mechanism (Nelson *et al.* 2012). Briefly, calpain can activate caspase-3, at least in part, by activating pro-apoptotic factors (e.g. tBid), leading to the release of cytochrome *c* from the mitochondria and the subsequent activation of caspase-9 (Nelson *et al.* 2012). Furthermore, caspase-3 can increase calpain activity by caspase-3-mediated degradation of calpastatin, an endogenous inhibitor of calpain activation (Nelson *et al.* 2012).

In addition to the role that active caspase-3 plays in protein degradation and muscle fibre atrophy, caspase-3 activation can promote DNA fragmentation and myonuclear apoptosis (Elliott, 2006; Smuder *et al.* 2011). Therefore, we investigated the role that mitochondrial ROS emission plays in DOX-induced myonuclear apoptosis in both cardiac and skeletal muscles. The results obtained confirm that DOX administration results in a significant increase in TUNEL-positive nuclei in both cardiac and skeletal muscles. Importantly, treatment with the mitochondrial-targeted anti-oxidant SS31 attenuated these DOX-induced increases in TUNEL-positive nuclei. Taken together, these findings show that increased mitochondrial ROS emission is an important contributor to DOX-induced activation of calpain, caspase-3 and myonuclear apoptosis, leading to a loss of nuclei from cardiac and skeletal muscles.

Calpain activation plays a contributory role in DOX-induced myopathy

Calpain is capable of cleaving numerous striated muscle proteins, including the important structural proteins titin and nebulin (Goll *et al.* 2003). Moreover, oxidative modification of sarcomeric proteins increases their susceptibility to degradation by calpain (Smuder *et al.* 2010) and, although some studies suggest that calpain contributes to DOX-induced myocardial dysfunction (Campos *et al.* 2011; Muller & Dhalla, 2012), the results of the present study provide the first *in vivo* evidence to support this prediction. Specifically, our results reveal that pharmacological inhibition of calpain activity attenuates the DOX-induced cardiac wall thinning and protects against DOX-induced decreases in LV systolic function. Furthermore, inhibition of calpain was sufficient to guard against DOX-induced atrophy in the diaphragm and locomotor skeletal muscles. Taken together, these results establish that the prevention of calpain activation provides a defence against DOX-induced atrophy and contractile dysfunction in both cardiac and skeletal muscles.

As discussed previously, an important finding from our studies is that active calpain is required for DOX-induced activation of caspase-3 in both heart and skeletal muscles. Indeed, when DOX-stimulated calpain activation was inhibited via the calpain inhibitor SJA 6017, caspase-3 was not activated in both cardiac and skeletal muscles. Note that we have previously demonstrated that SJA 6017 does not inhibit caspase-3 and therefore our finding that calpain activation is required to activate caspase-3 is not a result of off-target pharmacological effects (Nelson *et al.* 2012).

Conclusions

The present study provides evidence that mitochondrial ROS emission and calpain activation play important roles in DOX-induced myopathy in cardiac and skeletal muscles. Specifically, our results reveal that mitochondria are the dominant source of ROS production in the cardiac and skeletal muscle following DOX administration and that increased mitochondrial ROS emission is a required upstream signal for activating key proteases (i.e. calpain and caspase-3) in both heart and skeletal muscles following DOX administration. Our experiments also reveal that calpain activation is a requirement for DOX-induced myopathy in cardiac and skeletal muscles. Furthermore, active calpain is a requirement for DOX-induced activation of caspase-3 in both heart and skeletal muscles. Collectively, these novel findings provide important insight into the mechanisms responsible for DOX-induced damage to cardiac and skeletal muscles. Importantly, these results suggest that the administration of a mitochondrial-targeted anti-oxidant or inhibition of calpain may have therapeutic potential in protecting against DOX-induced myopathy in both heart and skeletal muscles. Nonetheless, future experiments are required to determine whether the use of mitochondrial-targeted molecules can protect against DOX-induced myopathy without diminishing the efficacy of DOX in the prevention of tumour growth.

References

Anderson EJ, Lustig ME, Boyle KE, Woodlief TL, Kane DA, Lin CT, Price JW, 3rd, Kang L, Rabinovitch PS, Szeto HH, Houmard JA, Cortright RN, Wasserman DH & Neufer PD (2009). Mitochondrial H_2O_2 emission and cellular redox state link excess fat intake to insulin resistance in both rodents and humans. *J Clin Invest* **119**, 573–581.

Anderson EJ & Neufer PD (2006). Type II skeletal myofibers possess unique properties that potentiate mitochondrial H(2)O(2) generation. *Am J Physiol Cell Physiol* **290**, C844–C851.

Anisimov VN, Bakeeva LE, Egormin PA, Filenko OF, Isakova EF, Manskikh VN, Mikhelson VM, Panteleeva AA, Pasyukova EG, Pilipenko DI, Piskunova TS, Popovich IG, Roshchina NV, Rybina OY, Saprunova VB, Samoylova TA, Semenchenko AV, Skulachev MV, Spivak IM, Tsybul'ko EA, Tyndyk ML, Vyssokikh MY, Yurova MN, Zabezhinsky MA & Skulachev VP (2008). Mitochondria-targeted plastoquinone derivatives as tools to interrupt execution of the aging pro-gram. 5. SkQ1 prolongs lifespan and prevents development of traits of senescence. *Biochemistry (Mosc)* **73**, 1329–1342.

Berthiaume JM & Wallace KB (2007). Adriamycin-induced oxidative mitochondrial cardiotoxicity. *Cell Biol Toxicol* **23**, 15–25.

Birk AV, Chao WM, Bracken C, Warren JD & Szeto HH (2014). Targeting mitochondrial cardiolipin and the cytochrome c/cardiolipin complex to promote electron transport and optimize mitochondrial ATP synthesis. *Br J Pharmacol* **171**, 2017–2028.

Birk AV, Liu S, Soong Y, Mills W, Singh P, Warren JD, Seshan SV, Pardee JD & Szeto HH (2013). The mitochondrial-targeted compound SS-31 re-energizes ischemic mitochondria by interacting with cardiolipin. *J Am Soc Nephrol* **24**, 1250–1261.

Campos EC, O'Connell JL, Malvestio LM, Romano MM, Ramos SG, Celes MR, Prado CM, Simoes MV & Rossi MA (2011). Calpain-mediated dystrophin disruption may be a potential structural culprit behind chronic doxorubicin-induced cardiomyopathy. *Eur J Pharmacol* **670**, 541–553.

Carvalho FS, Burgeiro A, Garcia R, Moreno AJ, Carvalho RA & Oliveira PJ (2014). Doxorubicin-induced cardiotoxicity: from bioenergetic failure and cell death to cardiomyopathy. *Med Res Rev* **34**, 106–135.

Chandran K, Aggarwal D, Migrino RQ, Joseph J, McAllister D, Konorev EA, Antholine WE, Zielonka J, Srinivasan S, Avadhani NG & Kalyanaraman B (2009). Doxorubicin inactivates myocardial cytochrome c oxidase in rats: cardioprotection by Mito-Q. *Biophys J* **96**, 1388–1398.

Childs AC, Phaneuf SL, Dirks AJ, Phillips T & Leeuwenburgh C (2002). Doxorubicin treatment in vivo causes cytochrome C release and cardiomyocyte apoptosis, as well as increased mitochondrial efficiency, superoxide dismutase activity, and Bcl-2:Bax ratio. *Cancer Res* **62**, 4592–4598.

Dai DF, Chiao YA, Marcinek DJ, Szeto HH & Rabinovitch PS (2014). Mitochondrial oxidative stress in aging and healthspan. *Longev Healthspan* **3**, 6.

Davies KJ & Doroshow JH (1986). Redox cycling of anthracyclines by cardiac mitochondria. I. Anthracycline radical formation by NADH dehydrogenase. *J Biol Chem* **261**, 3060–3067.

Doroshow JH (1983). Anthracycline antibiotic-stimulated superoxide, hydrogen peroxide, and hydroxyl radical production by NADH dehydrogenase. *Cancer Res* **43**, 4543–4551.

Doughan AK & Dikalov SI (2007). Mitochondrial redox cycling of mitoquinone leads to superoxide production and cellular apoptosis. *Antioxid Redox Signal* **9**, 1825–1836.

Elliott P (2006). Pathogenesis of cardiotoxicity induced by anthracyclines. *Semin Oncol* **33**, S2–S7.

Ferrans VJ (1978). Overview of cardiac pathology in relation to anthracycline cardiotoxicity. *Cancer Treat Rep* **62**, 955–961.

Fukiage C, Azuma M, Nakamura Y, Tamada Y, Nakamura M & Shearer TR (1997). SJA6017, a newly synthesized peptide aldehyde inhibitor of calpain: amelioration of cataract in cultured rat lenses. *Biochim Biophys Acta* **1361**, 304–312.

Gilliam LA, Ferreira LF, Bruton JD, Moylan JS, Westerblad H, St Clair DK & Reid MB (2009). Doxorubicin acts through tumor necrosis factor receptor subtype 1 to cause dysfunction of murine skeletal muscle. *J Appl Physiol* **107**, 1935–1942.

Gilliam LA, Fisher-Wellman KH, Lin CT, Maples JM, Cathey BL & Neufer PD (2013). The anticancer agent doxorubicin disrupts mitochondrial energy metabolism and redox balance in skeletal muscle. *Free Radic Biol Med* **65**, 988–996.

Gilliam LA, Moylan JS, Ann Callahan L, Sumandea MP & Reid MB (2011). Doxorubicin causes diaphragm weakness in murine models of cancer chemotherapy. *Muscle Nerve* **43**, 94–102.

Goll DE, Thompson VF, Li H, Wei W & Cong J (2003). The calpain system. *Physiol Rev* **83**, 731–801.

Goormaghtigh E, Huart P, Brasseur R & Ruysschaert JM (1986). Mechanism of inhibition of mitochondrial enzymatic complex I-III by adriamycin derivatives. *Biochim Biophys Acta* **861**, 83–94.

Goormaghtigh E, Huart P, Praet M, Brasseur R & Ruysschaert JM (1990). Structure of the adriamycin-cardiolipin complex. Role in mitochondrial toxicity. *Biophys Chem* **35**, 247–257.

Hayward R, Hydock D, Gibson N, Greufe S, Bredahl E & Parry T (2013). Tissue retention of doxorubicin and its effects on cardiac, smooth, and skeletal muscle function. *J Physiol Biochem* **69**, 177–187.

Ichikawa Y, Ghanefar M, Bayeva M, Wu R, Khechaduri A, Naga Prasad SV, Mutharasan RK, Naik TJ & Ardehali H (2014). Cardiotoxicity of doxorubicin is mediated through mitochondrial iron accumulation. *J Clin Invest* **124**, 617–630.

Jeyaseelan R, Poizat C, Wu HY & Kedes L (1997). Molecular mechanisms of doxorubicin-induced cardiomyopathy. Selective suppression of Reiske iron-sulfur protein, ADP/ATP translocase, and phosphofructokinase genes is associated with ATP depletion in rat cardiomyocytes. *J Biol Chem* **272**, 5828–5832.

Kang YJ, Chen Y, Yu A, Voss-McCowan M & Epstein PN (1997). Overexpression of metallothionein in the heart of transgenic mice suppresses doxorubicin cardiotoxicity. *J Clin Invest* **100**, 1501–1506.

Kavazis AN, Smuder AJ, Min K, Tumer N & Powers SK (2010). Short-term exercise training protects against doxorubicin-induced cardiac mitochondrial damage independent of HSP72. *Am J Physiol Heart Circ Physiol* **299**, H1515–H1524.

Kupina NC, Nath R, Bernath EE, Inoue J, Mitsuyoshi A, Yuen PW, Wang KK & Hall ED (2001). The novel calpain inhibitor SJA6017 improves functional outcome after delayed administration in a mouse model of diffuse brain injury. *J Neurotrauma* **18**, 1229–1240.

Lim CC, Zuppinger C, Guo X, Kuster GM, Helmes M, Eppenberger HM, Suter TM, Liao R & Sawyer DB (2004). Anthracyclines induce calpain-dependent titin proteolysis and necrosis in cardiomyocytes. *J Biol Chem* **279**, 8290–8299.

McClung JM, Kavazis AN, DeRuisseau KC, Falk DJ, Deering MA, Lee Y, Sugiura T & Powers SK (2007). Caspase-3 regulation of diaphragm myonuclear domain during mechanical ventilation-induced atrophy. *Am J Respir Crit Care Med* **175**, 150–159.

Messer JI, Jackman MR & Willis WT (2004). Pyruvate and citric acid cycle carbon requirements in isolated skeletal muscle mitochondria. *Am J Physiol Cell Physiol* **286**, C565–C572.

Min K, Smuder AJ, Kwon OS, Kavazis AN, Szeto HH & Powers SK (2011). Mitochondrial-targeted antioxidants protect skeletal muscle against immobilization-induced muscle atrophy. *J Appl Physiol* **111**, 1459–1466.

Montaigne D, Marechal X, Preau S, Baccouch R, Modine T, Fayad G, Lancel S & Neviere R (2011). Doxorubicin induces mitochondrial permeability transition and contractile dysfunction in the human myocardium. *Mitochondrion* **11**, 22–26.

Muller AL & Dhalla NS (2012). Role of various proteases in cardiac remodeling and progression of heart failure. *Heart Fail Rev* **17**, 395–409.

Myers CE, McGuire WP, Liss RH, Ifrim I, Grotzinger K & Young RC (1977). Adriamycin: the role of lipid peroxidation in cardiac toxicity and tumor response. *Science* **197**, 165–167.

Nelson WB, Smuder AJ, Hudson MB, Talbert EE & Powers SK (2012). Cross-talk between the calpain and caspase-3 proteolytic systems in the diaphragm during prolonged mechanical ventilation. *Crit Care Med* **40**, 1857–1863.

Pfeiffer K, Gohil V, Stuart RA, Hunte C, Brandt U, Greenberg ML & Schagger H (2003). Cardiolipin stabilizes respiratory chain supercomplexes. *J Biol Chem* **278**, 52873–52880.

Powers SK, Hudson MB, Nelson WB, Talbert EE, Min K, Szeto HH, Kavazis AN & Smuder AJ (2011*a*). Mitochondria-targeted antioxidants protect against mechanical ventilation-induced diaphragm weakness. *Crit Care Med* **39**, 1749–1759.

Powers SK, Kavazis AN & McClung JM (2007). Oxidative stress and disuse muscle atrophy. *J Appl Physiol (1985)* **102**, 2389–2397.

Powers SK, Smuder AJ & Criswell DS (2011*b*). Mechanistic links between oxidative stress and disuse muscle atrophy. *Antioxid Redox Signal* **15**, 2519–2528.

Powers SK, Smuder AJ & Judge AR (2012*a*). Oxidative stress and disuse muscle atrophy: cause or consequence? *Curr Opin Clin Nutr Metab Care* **15**, 240–245.

Powers SK, Wiggs MP, Duarte JA, Zergeroglu AM & Demirel HA (2012*b*). Mitochondrial signaling contributes to disuse muscle atrophy. *Am J Physiol Endocrinol Metab* **303**, E31–E39.

Reid MB (2008). Free radicals and muscle fatigue: Of ROS, canaries, and the IOC. *Free Radic Biol Med* **44**, 169–179.

Saido TC, Sorimachi H & Suzuki K (1994). Calpain: new perspectives in molecular diversity and physiological-pathological involvement. *FASEB J* **8**, 814–822.

Segal SS, White TP & Faulkner JA (1986). Architecture, composition, and contractile properties of rat soleus muscle grafts. *Am J Physiol Cell Physiol* **250**, C474–C479.

Sharma AK & Rohrer B (2004). Calcium-induced calpain mediates apoptosis via caspase-3 in a mouse photoreceptor cell line. *J Biol Chem* **279**, 35564–35572.

Singal PK, Iliskovic N, Li T & Kumar D (1997). Adriamycin cardiomyopathy: pathophysiology and prevention. *FASEB J* **11**, 931–936.

Singal PK, Li T, Kumar D, Danelisen I & Iliskovic N (2000). Adriamycin-induced heart failure: mechanism and modulation. *Mol Cell Biochem* **207**, 77–86.

Smuder AJ, Kavazis AN, Hudson MB, Nelson WB & Powers SK (2010). Oxidation enhances myofibrillar protein degradation via calpain and caspase-3. *Free Radic Biol Med* **49**, 1152–1160.

Smuder AJ, Kavazis AN, Min K & Powers SK (2011). Exercise protects against doxorubicin-induced oxidative stress and proteolysis in skeletal muscle. *J Appl Physiol* **110**, 935–942.

Tokarska-Schlattner M, Zaugg M, Zuppinger C, Wallimann T & Schlattner U (2006). New insights into doxorubicin-induced cardiotoxicity: the critical role of cellular energetics. *J Mol Cell Cardiol* **41**, 389–405.

vanNorren K, vanHelvoort A, Argiles JM, vanTuijl S, Arts K, Gorselink M, Laviano A, Kegler D, Haagsman HP & vander Beek EM (2009). Direct effects of doxorubicin on skeletal muscle contribute to fatigue. *Br J Cancer* **100**, 311–314.

Wallace KB (2007). Adriamycin-induced interference with cardiac mitochondrial calcium homeostasis. *Cardiovasc Toxicol* **7**, 101–107.

Whidden MA, Smuder AJ, Wu M, Hudson MB, Nelson WB & Powers SK (2010). Oxidative stress is required for mechanical ventilation-induced protease activation in the diaphragm. *J Appl Physiol* **108**, 1376–1382.

Wonders KY, Hydock DS, Greufe S, Schneider CM & Hayward R (2009). Endurance exercise training preserves cardiac function in rats receiving doxorubicin and the HER-2 inhibitor GW2974. *Cancer Chemother Pharmacol* **64**, 1105–1113.

Yamamoto Y, Hoshino Y, Ito T, Nariai T, Mohri T, Obana M, Hayata N, Uozumi Y, Maeda M, Fujio Y & Azuma J (2008). Atrogin-1 ubiquitin ligase is upregulated by doxorubicin via p38-MAP kinase in cardiac myocytes. *Cardiovasc Res* **79**, 89–96.

Yen HC, Oberley TD, Vichitbandha S, Ho YS & St Clair DK (1996). The protective role of manganese superoxide dismutase against adriamycin-induced acute cardiac toxicity in transgenic mice. *J Clin Invest* **98**, 1253–1260.

Zhao K, Zhao GM, Wu D, Soong Y, Birk AV, Schiller PW & Szeto HH (2004). Cell-permeable peptide antioxidants targeted to inner mitochondrial membrane inhibit mitochondrial swelling, oxidative cell death, and reperfusion injury. *J Biol Chem* **279**, 34682–34690.

Additional information

Competing interests

The SS peptides technology has been licensed for commercial development by the Cornell Research Foundation (CRF), and both CRF and Hazel H. Szeto have financial interests. Scott K. Powers and Hazel H. Szeto have filed a patent application for the protocol for the application of SS31 as an agent to protect against disuse skeletal muscle atrophy.

Author contributions

All authors approved the final version of the manuscript submitted for publication. All individuals designated as authors qualify for authorship and all those who qualify for authorship are listed. All authors participated in the conception and design of the experiments; collection, analysis and interpretation of data; and drafting of the article or revising it critically for important intellectual content.

Funding

No funding was received for these experiments.